

## C: Energy Conversion and Storage; Energy and Charge Transport

**Order-Disorder Transition in Kesterite CuZnSnS: Thermopower Enhancement via Electronic Band Structure Modification**

Eleonora Isotta, Binayak Mukherjee, Carlo Fanciulli, Nicola Maria Pugno, and Paolo Scardi

*J. Phys. Chem. C*, **Just Accepted Manuscript** • DOI: 10.1021/acs.jpcc.0c00886 • Publication Date (Web): 09 Mar 2020Downloaded from [pubs.acs.org](https://pubs.acs.org) on March 10, 2020**Just Accepted**

“Just Accepted” manuscripts have been peer-reviewed and accepted for publication. They are posted online prior to technical editing, formatting for publication and author proofing. The American Chemical Society provides “Just Accepted” as a service to the research community to expedite the dissemination of scientific material as soon as possible after acceptance. “Just Accepted” manuscripts appear in full in PDF format accompanied by an HTML abstract. “Just Accepted” manuscripts have been fully peer reviewed, but should not be considered the official version of record. They are citable by the Digital Object Identifier (DOI®). “Just Accepted” is an optional service offered to authors. Therefore, the “Just Accepted” Web site may not include all articles that will be published in the journal. After a manuscript is technically edited and formatted, it will be removed from the “Just Accepted” Web site and published as an ASAP article. Note that technical editing may introduce minor changes to the manuscript text and/or graphics which could affect content, and all legal disclaimers and ethical guidelines that apply to the journal pertain. ACS cannot be held responsible for errors or consequences arising from the use of information contained in these “Just Accepted” manuscripts.

1  
2  
3  
4  
5  
6  
7 **Order-Disorder Transition in Kesterite  $\text{Cu}_2\text{ZnSnS}_4$ :**  
8  
9  
10  
11 **Thermopower Enhancement via Electronic Band**  
12  
13  
14  
15 **Structure Modification**  
16  
17  
18  
19

20 *Eleonora Isotta,<sup>a,b</sup> Binayak Mukherjee,<sup>a</sup> Carlo Fanciulli,<sup>c</sup> Nicola M. Pugno,<sup>a,b,d,e</sup> and Paolo*  
21 *Scardi<sup>\*a</sup>*  
22  
23  
24  
25

26 <sup>a</sup>Department of Civil, Environmental and Mechanical Engineering, University of Trento, via  
27 Mesiano 77, 38123 Trento, Italy

29 <sup>b</sup>Laboratory of Bio-inspired, Bionic, Nano, Meta Materials & Mechanics, Department of Civil,  
30 Environmental and Mechanical Engineering, University of Trento, via Mesiano 77, 38123  
31 Trento, Italy

34 <sup>c</sup>National Research Council of Italy-Institute of Condensed Matter Chemistry and Technologies  
35 for Energy (CNR-ICMATE), Lecco Unit, via Previati 1/E, 23900 Lecco, Italy

38 <sup>d</sup>Ket-Lab, Edoardo Amaldi Foundation, Via del Politecnico snc, 00133 Rome, Italy

39 <sup>e</sup>School of Engineering and Materials Science, Queen Mary University of London, Mile End  
40 Road, London E1 4NS, UK  
41  
42  
43  
44  
45  
46  
47  
48  
49  
50  
51  
52  
53  
54  
55  
56  
57  
58  
59  
60

1  
2  
3 ABSTRACT  
4  
5  
6

7 The order-disorder transition of kesterite (CZTS,  $\text{Cu}_2\text{ZnSnS}_4$ ) from  $I-4$  to  $I-42m$  crystal  
8 structures has a marked effect on Seebeck coefficient, which displays a sharp enhancement at the  
9 transition temperature, around 533K. Considered to be detrimental for the performance of  
10 photovoltaic kesterite, the order-disorder transition appears to be beneficial for thermopower.  
11 Experimental data and *ab initio* calculations explain the origin of this enhancement: the increase  
12 of crystal symmetry in the disordered polymorph leads to a favorable electronic band structure  
13 characterized by flat and converged bands. At the transition, a sharp drop in mobility and  
14 increase in carrier concentration experimentally prove this mechanism of Seebeck enhancement.  
15 This, other than providing a new understanding of the material, can cast light on some profitable  
16 mechanisms to enhance the thermoelectric performance. Additionally, the increase in Seebeck  
17 provides an efficient tool to observe the transition and possibly to quantify disorder.  
18  
19  
20  
21  
22  
23  
24  
25  
26  
27  
28  
29  
30  
31  
32  
33  
34  
35  
36  
37  
38  
39  
40  
41  
42  
43  
44  
45  
46  
47  
48  
49  
50  
51  
52  
53  
54  
55  
56  
57  
58  
59  
60

## 1. Introduction

Kesterite (CZTS) is a p-type chalcogenide material with reference formula  $\text{Cu}_2\text{ZnSnS}_4$ . It has long been studied as absorber in thin film photovoltaic devices,<sup>1-3</sup> and recently deemed promising as a potential thermoelectric material,<sup>4-10</sup> valued for its intrinsically low thermal conductivity<sup>4</sup> and composition based on non-toxic, abundant and low-cost elements.<sup>11</sup> In its ordered and low temperature form, kesterite is reported having a tetragonal  $I-4$  crystal structure, while it was recently proved that a cubic  $F-43m$  low-temperature polymorph can be obtained for samples made by high-energy ball-milling, as an effect of a high disorder state of the cations.<sup>4,12</sup> This appears to be a metastable phase, since it transitions to the tetragonal polymorph on heating, as the temperature activates a reordering of the cations.<sup>4</sup> At around 533K, tetragonal kesterite faces a reversible order-disorder phase transition: cations in the intermediate Cu-Zn planes of the  $I-4$  structure ( $2c$  and  $2d$  Wyckoff positions) completely randomize their position (becoming  $4d$  Wyckoff position) thus transitioning to the tetragonal  $I-42m$  structure.<sup>5,13-15</sup> This transition has been studied in some detail in recent years, because disorder is considered detrimental for the photovoltaic performance of CZTS, as well as difficult to avoid. In fact, owing to the low formation energy of the  $\text{Cu}_{\text{Zn}}$  and  $\text{Zn}_{\text{Cu}}$  antisite defects,<sup>16,17</sup> a certain degree of disorder is inevitable in CZTS, even after extensive annealing treatments. Significant efforts have been made to quantify the degree of disorder and the subsequent loss in photovoltaic efficiency, rarely finding an ultimately suitable technique.<sup>5,14</sup> Nevertheless, for what concerns thermoelectric performance things proved to be different: the order-disorder transition has a marked and beneficial effect on the Seebeck coefficient.<sup>5</sup>



1  
2  
3 The aim of this work is to demonstrate experimentally and through *ab initio* calculations the  
4 physical origin of the increase in thermopower caused by the order-disorder transition of  
5 kesterite, which we connect with the crystal-symmetry induced modification of the electronic  
6 band structure. We also show how the degree of order of a sample affects the Seebeck  
7 coefficient.  
8  
9  
10  
11  
12  
13

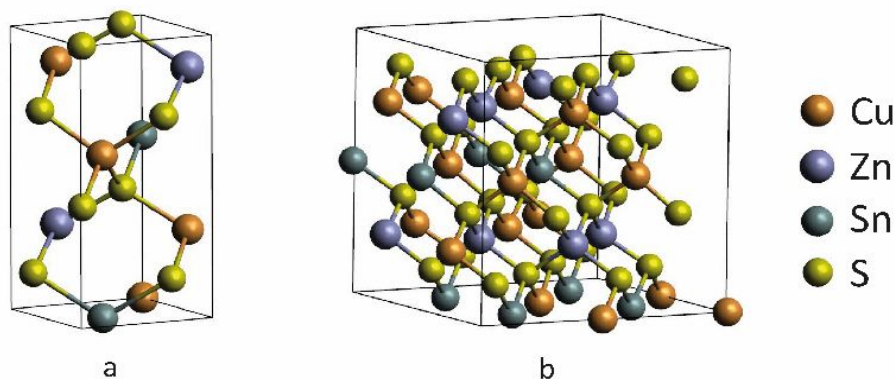
## 14 **2. Methods**

### 15 **2.1 Experimental**

16  
17  
18 Bulk kesterite sintered disks were produced according to previously described procedures,<sup>4,5</sup>  
19 starting from reactive ball milling of the elementary components, i.e., metals and sulfur in  
20 stoichiometric proportions, to obtain kesterite nanometric powders, then cold-pressed and  
21 thermally treated. Some of the samples undergone a quenching process in air, either starting from  
22 the sintering temperature of 560°C, or from a lower temperature reached with natural cooling, to  
23 room temperature. Absolute Seebeck coefficient measurements have been performed in 4-  
24 contact configuration and with Pt standard with a Linseis LZT Meter, in the temperature range  
25 320K-720K, with a temperature gradient of 10K. Carrier density and mobility have been  
26 measured with an MMR K-20 and an H-50 measurement systems. Results are obtained by a  
27 combined measurement of Hall effect and resistivity as a function of temperature. Resistivity is  
28 determined by the Van Der Pauw method using squared shaped samples with thickness below 1  
29 mm, providing an optimal geometrical ratio between surface and thickness. Hall effect  
30 measurements have been performed with a permanent-magnet field of 6270±10 G. The currents  
31 for testing have been set to values below 10 mA in order to prevent any thermal change in the  
32 samples. All the measurements are performed in vacuum, to prevent material degradation, and in  
33 the temperature range 300K-620K.  
34  
35  
36  
37  
38  
39  
40  
41  
42  
43  
44  
45  
46  
47  
48  
49  
50  
51  
52  
53  
54  
55  
56  
57  
58  
59  
60

## 2.2 Density Functional Theory (DFT) calculations

The ab initio electronic structure calculations with DFT have been performed using the plane wave basis set implemented in the Vienna ab initio simulation package (VASP).<sup>18,19</sup> The electron-exchange correlation functional was approximated using the Perdew-Burke-Ernzerhof (PBE)<sup>20</sup> form of the generalized gradient approximation (GGA). All calculations were performed with an energy cut-off of 300 eV. The ordered and disordered structures were modelled with 16 and 64 atom supercells respectively, visible in Figure 1, and the geometry was optimized with an 8x8x8 and 4x4x4 Monkhorst Pack (MP) k-mesh, respectively, centered at the  $\Gamma$  point, with Gaussian charge smearing in the order of 0.01 eV. The electronic degrees of freedom were relaxed until the change in the total free energy and energy eigenvalues were both smaller than  $10^{-6}$  eV. The disordered structure was generated by manually assigning a random Cu/Zn arrangement in the  $4d$  Wyckoff positions of the  $I-42m$  structure, keeping the overall stoichiometry balanced (Cu:Zn = 1:1 in  $4d$  sites). The bands were calculated along a high-symmetry path in the irreducible Brillouin zone obtained using the SeeK-path<sup>21</sup> tool, while the electronic density of states (*DoS*) was obtained using a dense 24x24x24 MP k-mesh for the 16-atom supercell and an 8x8x8 MP k-mesh for the 64-atom supercells.



1  
2  
3  
4  
5 **Figure 1.** Supercell crystal structures of kesterite used in DFT calculations: (a) ordered, s.g.  $I-4$   
6 and 16-atom cell; (b) disordered, s.g.  $I-42m$  and 64-atom supercell.  
7  
8  
9

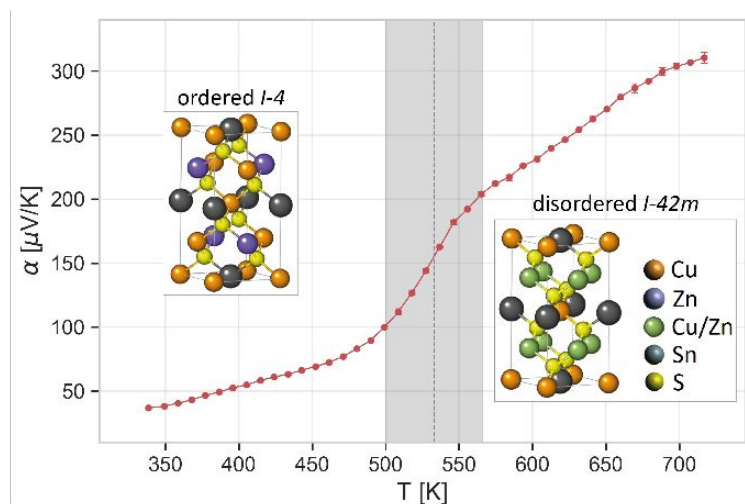
### 10 3. Results and discussion

#### 11 3.1 Thermoelectric properties

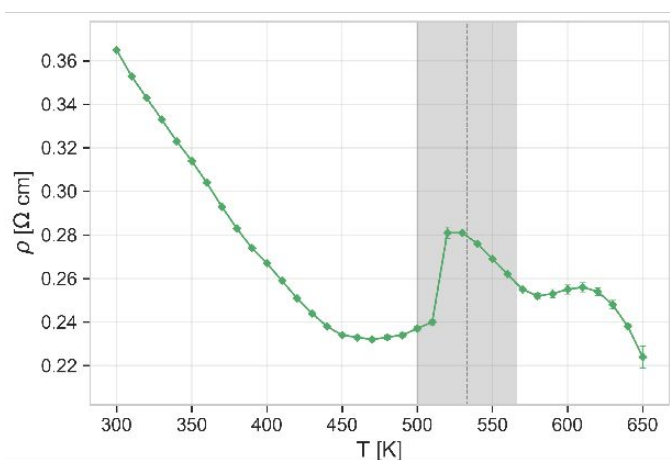
12  
13 The order-disorder phase transition of kesterite, from the ordered  $I-4$  to the disordered  
14  $I-42m$  tetragonal structures, has been reported at  $533\text{K} \pm 10\text{K}$ .<sup>13,14</sup> As shown by thermal  
15 analyses, it is a second-order and reversible transition,<sup>5</sup> and it consists of a full  
16 occupational disorder of Cu and Zn cations in the  $4d$  Wyckoff positions. This transition  
17 appears to have a beneficial role for thermoelectric CZTS. Indeed, the measurement of  
18 Seebeck coefficient, reproduced in Figure 2a, displays a sharp increase around the  
19 transition temperature.<sup>5</sup> Insets of Figure 2a show the ordered  $I-4$  crystal structure for the  
20 region below the transition temperature, where Cu and Zn occupy specific positions in the  
21 intermediate planes, and the disordered  $I-42m$  structure for the high-temperature region,  
22 where a unique position is considered to account for a mixed and random occupation of  
23 the two cations. We have put forward that this enhancement is due to a higher symmetry  
24 in the crystal structure of disordered CZTS.<sup>5</sup> Indeed, due to this loss of specificity in the  
25 positions of Cu and Zn, the disordered is a more symmetric structure. This can also be  
26 noticed by the additional 2-fold rotation axis and mirror plane specified in the space  
27 group  $I-42m$ .  
28  
29  
30  
31  
32  
33  
34  
35  
36  
37  
38  
39  
40  
41  
42  
43  
44  
45  
46  
47  
48  
49

50 Figure 2b shows the electrical resistivity measured in Van Der Pauw configuration, while  
51 Figure 2c displays the carrier concentration, measured via Hall effect on the same sample,  
52 and the carrier mobility, calculated from resistivity and carrier concentration data. Around  
53  
54  
55  
56  
57  
58  
59  
60

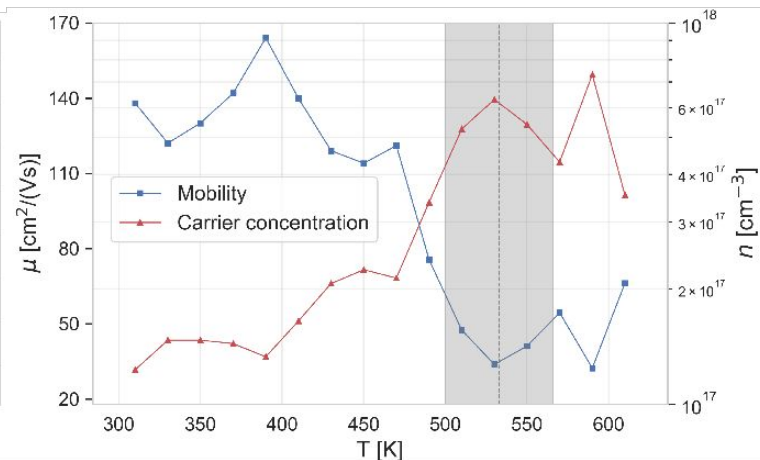
the order-disorder transition temperature we notice a substantial increase in carrier concentration, that nearly triples its values, and a corresponding decrease in mobility. We observe a kink in resistivity (Figure 2b) around the transition temperature. It is worth mentioning that literature data reports a smaller electronic bandgap  $E_g$  for disordered kesterite ( $\sim 1.50$  eV) with respect to ordered ( $\sim 1.67$  eV).<sup>15,22</sup>



a



b



c

**Figure 2.** (a) Absolute Seebeck coefficient  $\alpha$  (standard deviation is expressed with error bars) with insets showing the relevant kesterite crystal structures for each temperature region, namely ordered  $I-4$  in the low-temperature and disordered  $I-42m$  in the high-temperature zone. Data reproduced from Ref.<sup>5</sup> with permission from MDPI. (b) Electrical resistivity  $\rho$  (standard deviation is expressed with error bars), (c) and carrier mobility  $\mu$  and concentration  $n$  (in logarithmic scale) measured for a bulk CZTS sample. In the order-disorder transition region (highlighted in grey) it is possible to notice an increase in Seebeck coefficient and carrier concentration, and a corresponding drop in the mobility. This is attributed to band structure modifications: crystal-symmetry induced band convergence and reduction of curvature.

### 3.2 Electronic band structure

In order to provide a theoretical explanation for the experimentally observed changes in thermopower, electrical resistivity, carrier mobility and carrier concentration caused by the order-disorder transition, we performed *ab initio* band structure calculations for ordered (Figure 3a) and disordered (Figure 3b) kesterite. From these calculations we observe a threefold effect on the bands caused by the transition from the ordered to the disordered phase. Firstly, we see an increased convergence at the top of the valence band in the disordered phase, with the separation between the top three bands dropping from 0.139 eV ( $\sim 5.51$  kT, calculated at  $T = 298$ K) for the ordered phase to 0.072 eV ( $\sim 1.39$  kT, calculated at  $T = 600$ K) for the disordered. Secondly, we observe a significant reduction in curvature (flattening) at the top of the valence band in the disordered phase compared to the ordered. Finally, we observe a decrease in the band gap going from the ordered to the disordered phase, though it must be considered that the exchange-correlation functional in GGA is known to strongly underestimate the band gap. While more sophisticated calculations using hybrid functionals do provide a better estimation of the band gap, they become prohibitively expensive in terms of computational resources, particularly for larger supercells such as the disordered structures. It may be assumed that the errors for similar systems are similar and cancel out in comparative studies, the accuracy of the calculations being validated by their agreement with experiments. The effect of an increased band convergence and a reduced curvature due to higher disorder in the crystal structure is evidenced also by the density of states (*DoS*), presented in Figure 3c, which is higher at the top of the valence band, with steeper slope of *DoS* (and of

$\ln(DoS)$ , in the inset) for the disordered phase with respect to the ordered. The asymmetry of the  $DoS$  with respect to the Fermi level is consistent with the p character of the material. In the Supporting Information, the extended band structures are visible, as well as the band structures for a partially disordered sample and another configuration of disorder, to confirm and generalize the validity of the DFT results.

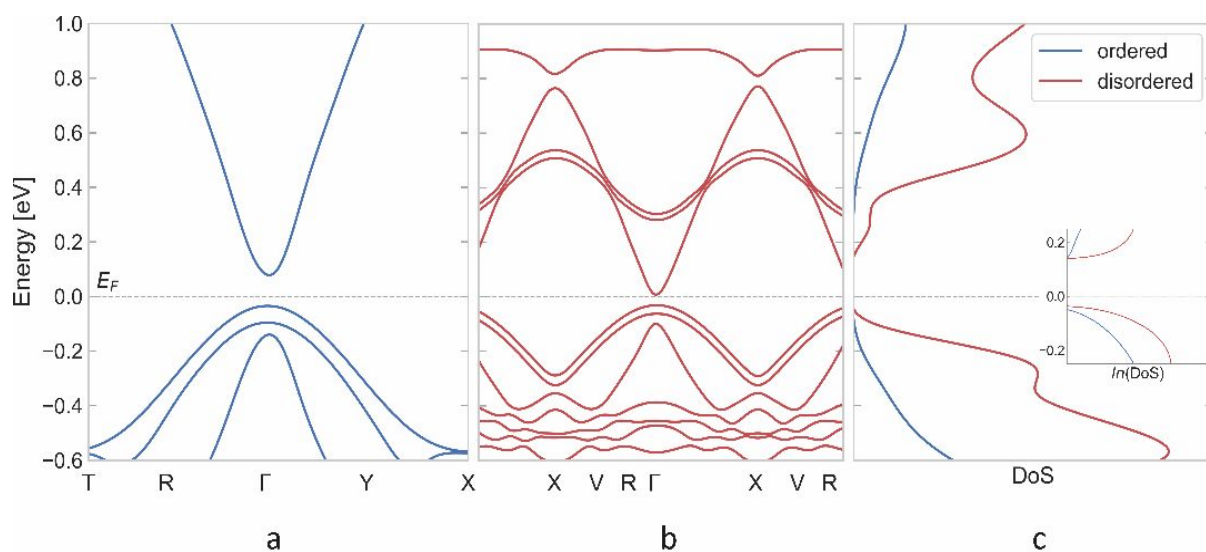


**Figure 3.** Band structures for ordered (a), and disordered (b) kesterite. Panel (c) displays the density of states  $DoS$ , with inset showing the natural logarithm of the  $DoS$ . With an increase of disorder, the top valence bands tend to converge and reduce their curvature, the bandgap narrows, while  $DoS$  and  $\ln(DoS)$  get higher and steeper. We believe this band structure modification is at the origin of the difference in electrical properties. The Fermi energy is set to 0 eV in each case. X-axis is on the same scale in k-space for (a) and (b).

### 3.3 Order-disorder transition: crystal symmetry induces band convergence and flatness

The thermopower is directly proportional to the density of state effective mass  $m_{DoS}^* = N_V^{2/3} m_i^*$ , where  $N_V$  is the band degeneracy and  $m_i^*$  is the inertial effective mass of charge carriers along the conduction direction.<sup>23</sup> It has been pointed out in the literature that there may be a connection between an increase in the symmetry of a crystal structure and an

1  
2  
3 improved band convergence.<sup>24–26</sup> We believe the order-disorder transition of CZTS to be  
4  
5 an example of this behavior: the higher crystal symmetry causes an increase in the  
6  
7 electronic band degeneracy  $N_V$ , as proved by DFT, thus justifying the sharp growth in the  
8  
9 experimentally observed Seebeck coefficient. We attribute the observed increase in  
10  
11 carrier concentration (Figure 2b) both to the decrease in  $E_g$  and to the convergence of  
12  
13 bands. In fact, were it due to a narrower bandgap alone, we would expect a corresponding  
14  
15 decrease in thermopower and electrical resistivity, while experimental data shows that  
16  
17 thermopower increases with the transition whereas resistivity does not decrease. A higher  
18  
19 band convergence could instead explain why we observe an enhancement of Seebeck  
20  
21 despite the increase in carrier concentration. Resistivity displays a sharp upwards kink  
22  
23 around the transition temperature, and then smoothly decreases to reach values in the  
24  
25 order of those obtained prior to the transition. This is also in contradiction with the  
26  
27 increased carrier concentration and can only be explained with the observed sharp drop in  
28  
29 mobility, which in this case we associate to a carrier localization due to band  
30  
31 convergence. In many literature cases, a pronounced decrease in mobility is associated to  
32  
33 an enhancement of thermopower,<sup>27</sup> along with a steeper  $DoS$  as expressed by Mott's  
34  
35 formula.<sup>28</sup> Moreover, from *ab initio* calculations we observe a reduced curvature in the  
36  
37 valence bands, which is in agreement with an increased  $m_I^*$  and decreased mobility.  
38  
39 Indeed, the movement of cations and the concurring rearrangement of covalent bonds  
40  
41 happening during the transition might have promoted a higher number of available energy  
42  
43 levels (therefore higher carrier concentration) but more localized (causing the drop in  
44  
45 mobility and the increase in Seebeck). This, contrary to what reported for other  
46  
47 systems,<sup>29,30</sup> seems to not extensively penalize electrical resistivity owing to the  
48  
49  
50  
51  
52  
53  
54  
55  
56  
57  
58  
59  
60

1  
2  
3 simultaneous increase in carrier concentration caused by band convergence. The  $DoS$ ,  
4 being higher for the disordered phase, highlights the higher availability of valence states  
5 close to the Fermi level and their higher occupation, associated to the reduced bandgap.  
6  
7 The trend of the logarithm of the density of states (shown in the inset of Figure 3c) is  
8 steeper at the top of the valence band for the disordered polymorph, in agreement with the  
9 higher thermopower provided for by Mott's formula.<sup>28</sup> Furthermore, a sharper asymmetry  
10 of the  $DoS$  with respect to the Fermi level is found which is consistent with the p-type  
11 nature and is typically associated with an increase in Seebeck.<sup>28</sup> In general, the DFT  
12 calculations are in good agreement with the experimental results. It is evident that the  
13 described phenomenon is dominated by band features (flatness and degeneracy), which is  
14 also supported by the low value of carrier concentration (in the order of  $10^{17}$   $\text{cm}^{-3}$ ) and  
15 can explain why we observe a decoupling of the thermopower and resistivity trends.  
16  
17 These results provide experimental and theoretical proof that favorable band structure and  
18 the subsequent enhancement of thermoelectric properties can be achieved with an  
19 increase in crystal symmetry.  
20  
21  
22  
23  
24  
25  
26  
27  
28  
29  
30  
31  
32  
33  
34  
35  
36

### 3.4 Seebeck as a method to observe the transition and estimate the degree of order

37  
38  
39  
40

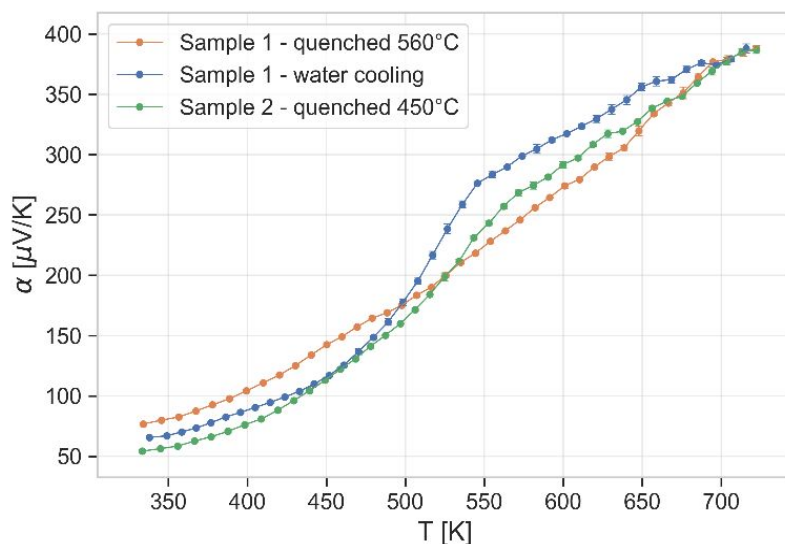
41 In the photovoltaic community, much research has been performed on methods to  
42 determine the degree of order in kesterite samples, as the lower bandgap of the disordered  
43 phase is deemed responsible for open-circuit voltage losses, thus undermining the solar-  
44 cell efficiency.<sup>13</sup> However, the search for a suitable and convenient technique, able to  
45 observe a clear difference between samples with different degrees of order, has proved a  
46 complex challenge. In fact, X-ray diffraction is not suitable for observing Cu-Zn disorder,  
47 because  $\text{Cu}^+$  and  $\text{Zn}^{2+}$  are isoelectronic and appear identical to X-rays. Other proposed  
48  
49  
50  
51  
52  
53  
54  
55  
56  
57  
58  
59  
60



1  
2  
3 methods include Raman spectroscopy, through the quantification of the relative intensity  
4 of secondary peaks,<sup>13,14,31,32</sup> optical measurements,<sup>15,22</sup> solid-state nuclear magnetic  
5 resonance<sup>33</sup> and neutron scattering<sup>34</sup>. In this context, we tentatively propose the Seebeck  
6 measurement as an alternative technique, as it proves efficient in observing the Cu-Zn  
7 transition of kesterite and sensitive to the degree of order in the sample. Indeed, we have  
8 experimentally observed that according to the level of order in the crystal structure at the  
9 beginning of the measurement, the transition appears in a different way. Figure 4 shows  
10 the trends of Seebeck coefficient for some of our CZTS samples characterized by  
11 different thermal histories, which is known to influence the degree of order.<sup>13,14</sup> Sample 1  
12 has been obtained by quenching right after the sintering process, at 560°C. This has been  
13 done to quench the fully disordered state of the crystal structure, and indeed the sample,  
14 on following heating, exhibits a flat trend of Seebeck coefficient, proving that no  
15 transition occurs.<sup>5</sup> A second measurement was then performed on the same sample after  
16 letting it to slowly cool down to ambient temperature (water cooling, ~ 2 h long). Sample  
17 2 has instead been obtained by allowing it to naturally cool down to 450°C after the  
18 thermal treatment, and then suddenly quenched to room temperature. The measurement of  
19 Seebeck coefficient displays a small increase around the transition temperature, pointing  
20 out that the sample was in a partly disordered state. These measurements point out that  
21 the degree of order can influence the behavior of Seebeck coefficient. Several research  
22 groups working on thermoelectric CZTS have reported different trends for Seebeck: some  
23 of them present a flat curve, that apparently does not display the order-disorder  
24 transition;<sup>6,7</sup> Sharma *et al.*, instead, report trends where an increase is visible around the  
25 transition temperature.<sup>9,10</sup> Based on the present results, the reason for this inconsistency of  
26  
27  
28  
29  
30  
31  
32  
33  
34  
35  
36  
37  
38  
39  
40  
41  
42  
43  
44  
45  
46  
47  
48  
49  
50  
51  
52  
53  
54  
55  
56  
57  
58  
59  
60

1  
2  
3 experimental results can be ascribed to different degree of order, as samples from the  
4 literature have diverse production routes and thermal histories, therefore being different in  
5  
6 literature have diverse production routes and thermal histories, therefore being different in  
7  
8 terms of ordering kinetics. Moreover, the band structure for a partially disordered sample,  
9  
10 shown in Figure S3a of the Supporting Information, exhibits an intermediate behavior with  
11  
12 respect to the ordered and fully disordered one, with a closer similarity to the latter. This is  
13  
14 consistent with the definition of random occupation of Cu and Zn cations for the disordered  
15  
16 structure, which will also include some narrow regions of order.  
17  
18

19  
20 Nevertheless, this dependence could be exploited to retrieve information on the sample,  
21  
22 here just qualitatively illustrated. Through a suitable empirical calibration with other  
23  
24 techniques or a suitable theoretical model, thermopower could be used to retrieve an order  
25  
26 parameter and to estimate the degree of order in a sample.  
27  
28  
29



30  
31  
32  
33  
34  
35  
36  
37  
38  
39  
40  
41  
42  
43  
44  
45  
46  
47  
48  
49 **Figure 4.** Absolute Seebeck coefficient  $\alpha$  for some CZTS samples: quenched from 560°C  
50 to preserve the disordered state, for the same sample after water cooling, and for a second  
51 sample, characterized by an intermediate disorder state.  
52

#### 53 4. Conclusions

54  
55  
56  
57  
58  
59  
60

1  
2  
3 The order-disorder transition of kesterite from ordered *I-4* to disordered *I-42m* crystal  
4 structures leads to a beneficial effect on thermopower that presents an increase around the  
5 transition temperature of 533K,<sup>5</sup> conversely to what happens for photovoltaic kesterite for  
6 which the transition is deemed detrimental for the performance.<sup>14</sup> In this work, we have  
7 demonstrated that the mechanism at the origin of this enhancement of Seebeck coefficient  
8 is an improved electronic band structure. DFT calculations show more converged and  
9 flatter bands for the disordered polymorph, which lead to an increased carrier  
10 concentration and a decreased mobility, confirmed by experimental data. A higher crystal  
11 symmetry for the disordered structure is deemed responsible for the improved band  
12 degeneracy, which in turn leads to a higher density of states effective mass and enhanced  
13 thermopower. Electrical resistivity, differently from what commonly occurs,<sup>29,30</sup> is not  
14 penalized by the low mobility due to the concurrent high carrier concentration originated  
15 from band convergence. These results, besides providing a new understanding of the  
16 studied material, can cast light on some profitable mechanisms to enhance the  
17 thermoelectric performance. Additionally, the measurement of Seebeck coefficient  
18 proved to be a simple and efficient way to observe the order-disorder transition of  
19 kesterite; as shown in this work, a different degree of order in the crystal structure causes  
20 the increase of Seebeck at the order-disorder transition to vary. This dependence could be  
21 exploited to estimate the degree of order in a sample, which has always been considered  
22 difficult to attribute due to the low sensitivity of other proposed methods.<sup>13,33</sup>  
23  
24 Furthermore, it could explain the difference found in the literature for CZTS in the trends  
25 of Seebeck coefficient, especially where the order-disorder transition is not explicitly  
26 observed or identified.<sup>6,7,9,10</sup>  
27  
28  
29  
30  
31  
32  
33  
34  
35  
36  
37  
38  
39  
40  
41  
42  
43  
44  
45  
46  
47  
48  
49  
50  
51  
52  
53  
54  
55  
56  
57  
58  
59  
60

1  
2  
3  
4  
5 ASSOCIATED CONTENT  
6  
7

8 **Supporting Information.** Additional DFT calculations for other configurations of disordered  
9 kesterite (PDF).  
10  
11  
12

13  
14 AUTHOR INFORMATION  
15

16  
17 **Corresponding Author**  
18

19 \*Email: [paolo.scardi@unitn.it](mailto:paolo.scardi@unitn.it); Tel: +39 0461 282417; Address: 38123 via Mesiano 77, Trento,  
20 Italy  
21  
22  
23

24  
25 **Author Contributions**  
26

27 The manuscript was written through contributions of all authors. All authors have given approval  
28 to the final version of the manuscript.  
29  
30  
31

32  
33 ACKNOWLEDGMENT  
34

35  
36  
37 This research was funded by the Autonomous Province of Trento, within the framework  
38 of the programmatic Energy Action 2015–2017. The computational time was provided by  
39 CINECA - Italian Supercomputing Facility, with the project CZTS - HP10CONX70.  
40  
41

42 N.M.P. is supported by the European Commission under the Graphene Flagship Core 2  
43 grant No. 785219 (WP14, “Composites”), the FET Proactive (“Neurofibres”) grant No.  
44 732344, the FET Open (Boheme) grant No. 863179 as well as by the Italian Ministry of  
45 Education, University and Research (MIUR) under the “Departments of Excellence”  
46 grant L. 232/2016, the ARS01- 01384-PROSCAN and the PRIN-20177TTP3S grants.  
47  
48  
49  
50  
51  
52  
53  
54  
55  
56  
57  
58  
59  
60

## REFERENCES

- (1) Katagiri, H.; Jimbo, K.; Yamada, S.; Kamimura, T.; Maw, W. S.; Fukano, T.; Ito, T.; Motohiro, T. Enhanced Conversion Efficiencies of Cu<sub>2</sub>ZnSnS<sub>4</sub>-Based Thin Film Solar Cells by Using Preferential Etching Technique. *Appl. Phys. Express* **2008**, *1* (4), 0412011–0412012. <https://doi.org/10.1143/APEX.1.041201>.
- (2) Ataollahi, N.; Malerba, C.; Ciancio, R.; Edla, R.; Scardi, P.; Cappelletto, E.; Di Maggio, R. Control of Composition and Grain Growth in Cu<sub>2</sub>ZnSnS<sub>4</sub> Thin Films from Nanoparticle Inks. *Thin Solid Films* **2019**, *674*, 12–21. <https://doi.org/10.1016/j.tsf.2019.02.004>.
- (3) Syafiq, U.; Ataollahi, N.; Maggio, R. Di; Scardi, P. Solution-Based Synthesis and Characterization of Cu<sub>2</sub>ZnSnS<sub>4</sub> (CZTS) Thin Films. *Molecules* **2019**, *24* (19), 3454. <https://doi.org/10.3390/molecules24193454>.
- (4) Isotta, E.; Pugno, N. M.; Scardi, P. Nanostructured Kesterite (Cu<sub>2</sub>ZnSnS<sub>4</sub>) for Applications in Thermoelectric Devices. *Powder Diffr.* **2019**, *0* (0), 2–7. <https://doi.org/10.1017/S0885715619000277>.
- (5) Isotta, E.; Fanciulli, C.; Pugno, N. M.; Scardi, P. Effect of the Order-Disorder Transition on the Seebeck Coefficient of Nanostructured Thermoelectric Cu<sub>2</sub>ZnSnS<sub>4</sub>. *Nanomaterials* **2019**, *9* (5), 762. <https://doi.org/10.3390/nano9050762>.
- (6) Liu, M. L.; Huang, F. Q.; Chen, L. D.; Chen, I. W. A Wide-Band-Gap p -Type Thermoelectric Material Based on Quaternary Chalcogenides of Cu<sub>2</sub>ZnSnQ<sub>4</sub>(Q=S,Se). *Appl. Phys. Lett.* **2009**, *94* (20), 202103. <https://doi.org/10.1063/1.3130718>.
- (7) Yang, H.; Jauregui, L. A.; Zhang, G.; Chen, Y. P.; Wu, Y. Non-Toxic and Abundant Copper Zinc Tin Sulfide Nanocrystals for Potential High Temperature Thermoelectric Energy Harvesting. *Nano Lett.* **2012**. <https://doi.org/10.1021/nl201718z>.
- (8) Kumar, S.; Ansari, M. Z.; Khare, N. Influence of Compactness and Formation of Metallic Secondary Phase on the Thermoelectric Properties of Cu<sub>2</sub>ZnSnS<sub>4</sub> Thin Films. *Thin Solid Films* **2018**, *645*, 300–304. <https://doi.org/10.1016/j.tsf.2017.11.001>.
- (9) Sharma, S. D.; Neeleshwar, S. Thermoelectric Properties of Hot Pressed CZTS Micro

- Spheres Synthesized by Microwave Method. *MRS Adv.* **2018**, *3* (24 (Energy and Sustainability)), 1373–1378. <https://doi.org/10.1557/adv.2018>.
- (10) Sharma, S. D.; Khasimsaheb, B.; Chen, Y. Y.; Neeleshwar, S. Enhanced Thermoelectric Performance of  $\text{Cu}_2\text{ZnSnS}_4$  ( CZTS ) by Incorporating Ag Nanoparticles. *Ceram. Int.* **2019**, *45* (2), 2060–2068. <https://doi.org/10.1016/j.ceramint.2018.10.109>.
- (11) Adachi, S. *Earth-Abundant Materials for Solar Cells*; 2015.
- (12) Kapusta, K.; Drygas, M.; Janik, J. F.; Jelen, P.; Bucko, M. M.; Olejniczak, Z. From Magnetic Cubic Pre-Kesterite to Semiconducting Tetragonal Kesterite  $\text{Cu}_2\text{ZnSnS}_4$  Nanopowders via the Mechanochemically Assisted Route. *J. Alloys Compd.* **2019**, *770*, 981–988. <https://doi.org/10.1016/j.jallcom.2018.08.135>.
- (13) Scragg, J. J. S.; Choubrac, L.; Lafond, A.; Ericson, T.; Platzer-Björkman, C. A Low-Temperature Order-Disorder Transition in  $\text{Cu}_2\text{ZnSnS}_4$  Thin Films. *Appl. Phys. Lett.* **2014**, *104* (041911), 041911. <https://doi.org/10.1063/1.4863685>.
- (14) Scragg, J. J. S.; Larsen, J. K.; Kumar, M.; Persson, C.; Sandler, J.; Siebentritt, S. Cu–Zn Disorder and Band Gap Fluctuations in  $\text{Cu}_2\text{ZnSn}(\text{S},\text{Se})_4$ : Theoretical and Experimental Investigations. *Phys. Status Solidi B* **2016**, *253* (2), 247–254. <https://doi.org/10.1002/pssb.201552530>.
- (15) Valentini, M.; Malerba, C.; Menchini, F.; Tedeschi, D.; Polimeni, A.; Capizzi, M.; Mittiga, A. Effect of the Order-Disorder Transition on the Optical Properties of  $\text{Cu}_2\text{ZnSnS}_4$ . *Appl. Phys. Lett.* **2016**, *108*, 211909. <https://doi.org/10.1063/1.4952973>.
- (16) Chen, S.; Gong, X. G.; Walsh, A.; Wei, S. Defect Physics of the Kesterite Thin-Film Solar Cell Absorber. **2010**, *96*, 021902. <https://doi.org/10.1063/1.3275796>.
- (17) Chen, S.; Walsh, A.; Gong, X.; Wei, S. Classification of Lattice Defects in the Kesterite  $\text{Cu}_2\text{ZnSnS}_4$  and  $\text{Cu}_2\text{ZnSnSe}_4$  Earth-Abundant Solar Cell Absorbers. *Adv. Mater.* **2013**, No. 25, 1522–1539. <https://doi.org/10.1002/adma.201203146>.
- (18) Kresse, G.; Furthmüller, J. Efficient Iterative Schemes for Ab Initio Total-Energy Calculations Using a Plane-Wave Basis Set. *Phys. Rev. B - Condens. Matter Mater. Phys.* **1996**, *54* (16), 11169–11186. <https://doi.org/10.1103/PhysRevB.54.11169>.
- (19) Kresse, G.; Furthmüller, J. Efficiency of Ab-Initio Total Energy Calculations for Metals and Semiconductors Using a Plane-Wave Basis Set. *Comput. Mater. Sci.* **1996**, *6* (1), 15–50. [https://doi.org/10.1016/0927-0256\(96\)00008-0](https://doi.org/10.1016/0927-0256(96)00008-0).

- 1  
2  
3 (20) Perdew, J. P.; Burke, K.; Ernzerhof, M. Generalized Gradient Approximation Made  
4 Simple. *Phys. Rev. Lett.* **1996**, *77* (18), 3865–3868.  
5 <https://doi.org/10.1103/PhysRevLett.77.3865>.  
6  
7  
8 (21) Hinuma, Y.; Pizzi, G.; Kumagai, Y.; Oba, F.; Tanaka, I. Band Structure Diagram Paths  
9 Based on Crystallography. *Comput. Mater. Sci.* **2017**, *128*, 140–184.  
10 <https://doi.org/10.1016/j.commatsci.2016.10.015>.  
11  
12  
13 (22) Malerba, C.; Valentini, M.; Mittiga, A. Cation Disorder in Cu<sub>2</sub>ZnSnS<sub>4</sub> Thin Films : Effect  
14 on Solar Cell Performances. *Sol. RRL* **2017**, *1*, 1700101.  
15 <https://doi.org/10.1002/solr.201700101>.  
16  
17  
18 (23) Kittel, C. *Introduction to Solid State Physics-8th Edition*; 2005.  
19 <https://doi.org/10.1119/1.1934457>.  
20  
21  
22 (24) Zeier, W. G.; Zhu, H.; Gibbs, Z. M.; Ceder, G.; Tremel, W.; Snyder, G. J. Band  
23 Convergence in the Non-Cubic Chalcopyrite Compounds Cu<sub>2</sub>MGeSe<sub>4</sub>. *J. Mater. Chem. C*  
24 **2014**, *2* (47), 10189–10194. <https://doi.org/10.1039/c4tc02218a>.  
25  
26  
27 (25) Zeier, W. G. New Tricks for Optimizing Thermoelectric Materials. *Curr. Opin. Green*  
28 *Sustain. Chem.* **2017**, *4*, 23–28. <https://doi.org/10.1016/j.cogsc.2017.02.003>.  
29  
30  
31 (26) Zhang, Q.; Song, Q.; Wang, X.; Sun, J.; Zhu, Q.; Dahal, K.; Lin, X.; Cao, F.; Zhou, J.;  
32 Chen, S.; et al. Deep Defect Level Engineering : A Strategy of Optimizing the Carrier  
33 Concentration for High Thermoelectric Performance. *Energy Environ. Sci.* **2018**, *11*, 933–  
34 940. <https://doi.org/10.1039/C8ee00112j>.  
35  
36  
37 (27) Sun, P.; Wei, B.; Zhang, J.; Tomczak, J. M.; Strydom, A. M.; Søndergaard, M.; Iversen,  
38 B. B.; Steglich, F. Large Seebeck Effect by Charge-Mobility Engineering. *Nat. Commun.*  
39 **2015**, *6* (May), 1–5. <https://doi.org/10.1038/ncomms8475>.  
40  
41  
42 (28) Mott, N. F.; Jones, H. The Theory of the Properties of Metals and Alloys. *Journal of*  
43 *Chemical Education*. 1936, p 99. <https://doi.org/10.1021/ed014p99>.  
44  
45  
46 (29) Pei, Y.; Wang, H.; Snyder, G. J. Band Engineering of Thermoelectric Materials. *Adv.*  
47 *Mater.* **2012**, *24* (46), 6125–6135. <https://doi.org/10.1002/adma.201202919>.  
48  
49  
50 (30) Pei, Y.; Lalonde, A. D.; Wang, H.; Snyder, G. J. Low Effective Mass Leading to High  
51 Thermoelectric Performance. *Energy Environ. Sci.* **2012**, *5* (7), 7963–7969.  
52 <https://doi.org/10.1039/c2ee21536e>.  
53  
54  
55 (31) Rudisch, K.; Ren, Y.; Platzer-Bjorkman, C.; Scragg, J. Order-Disorder Transition in B-

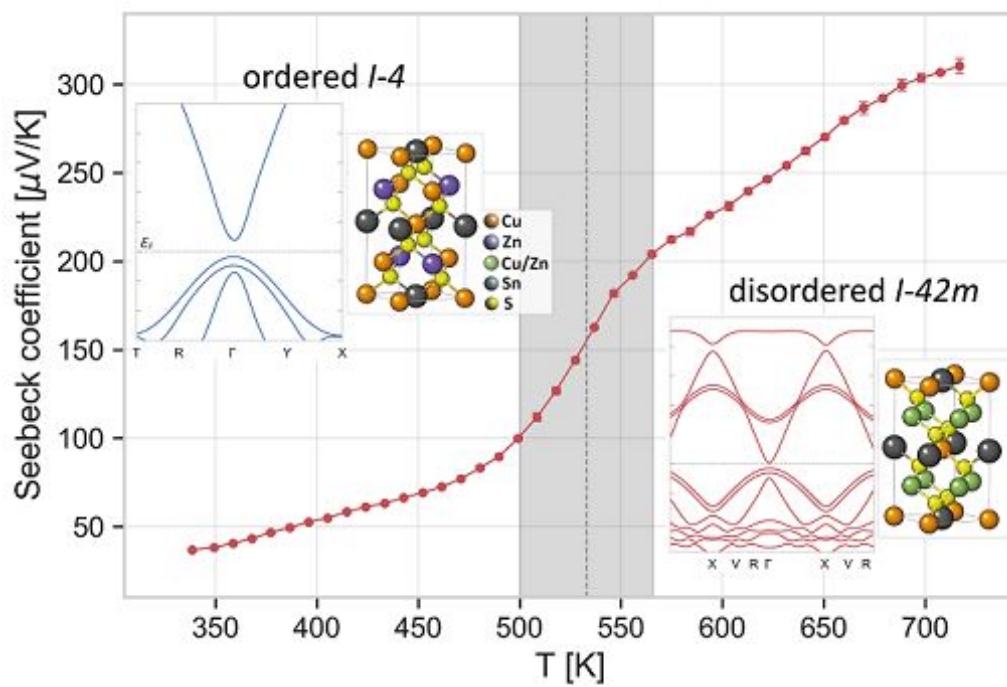
1  
2  
3 Type Cu<sub>2</sub>ZnSnS<sub>4</sub> and Limitations of Ordering through Thermal Treatments. *Appl. Phys. Lett.* **2016**, No. 108, 231902. <https://doi.org/10.1063/1.4953349>.  
4  
5  
6

7 (32) Rudisch, K.; Davydova, A.; Platzer-björkman, C. The Effect of Stoichiometry on Cu-Zn  
8 Ordering Kinetics in Cu<sub>2</sub>ZnSnS<sub>4</sub> Thin Films. **2018**, 161558 (October 2017).  
9 <https://doi.org/10.1063/1.5010081>.  
10  
11

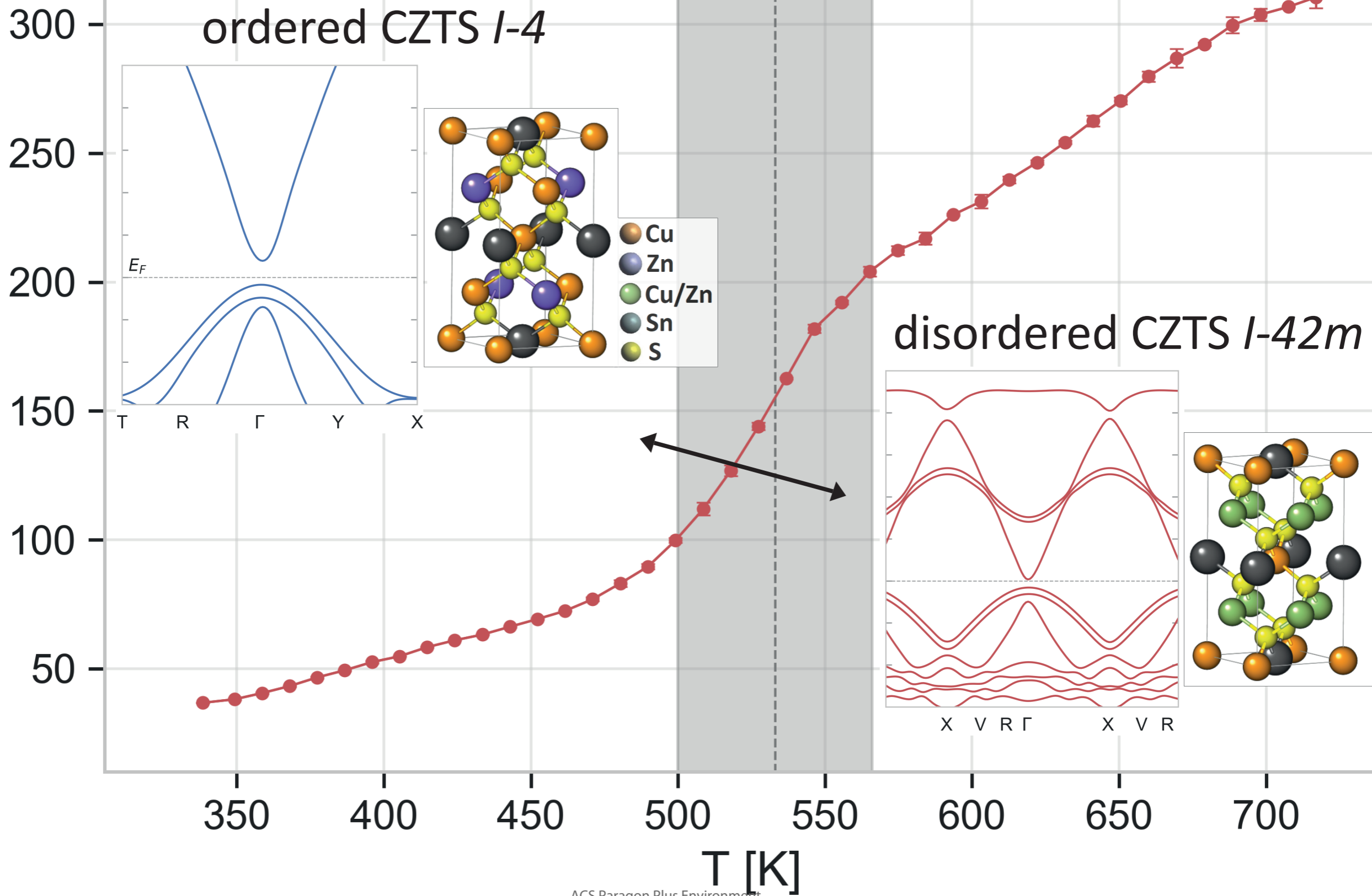
12 (33) Paris, M.; Lafond, A.; Guillot-deudon, C. Solid-State NMR and Raman Spectroscopy To  
13 Address the Local Structure of Defects and the Tricky Issue of the Cu/Zn Disorder in Cu-  
14 Poor, Zn-Rich CZTS Materials. *Inorg. Chem.* **2014**, 53, 8646–8653.  
15 <https://doi.org/10.1021/ic5012346>.  
16  
17

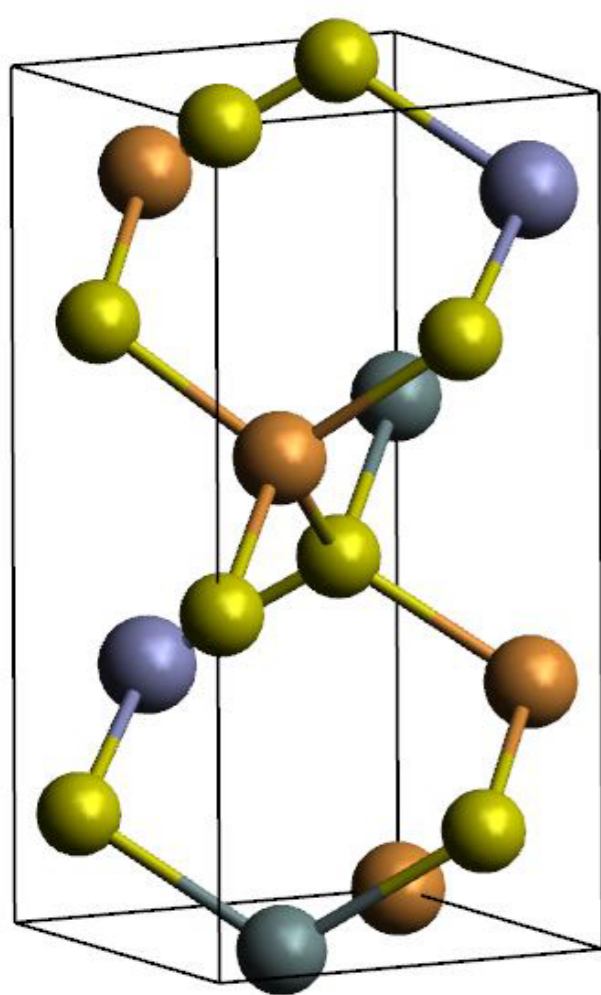
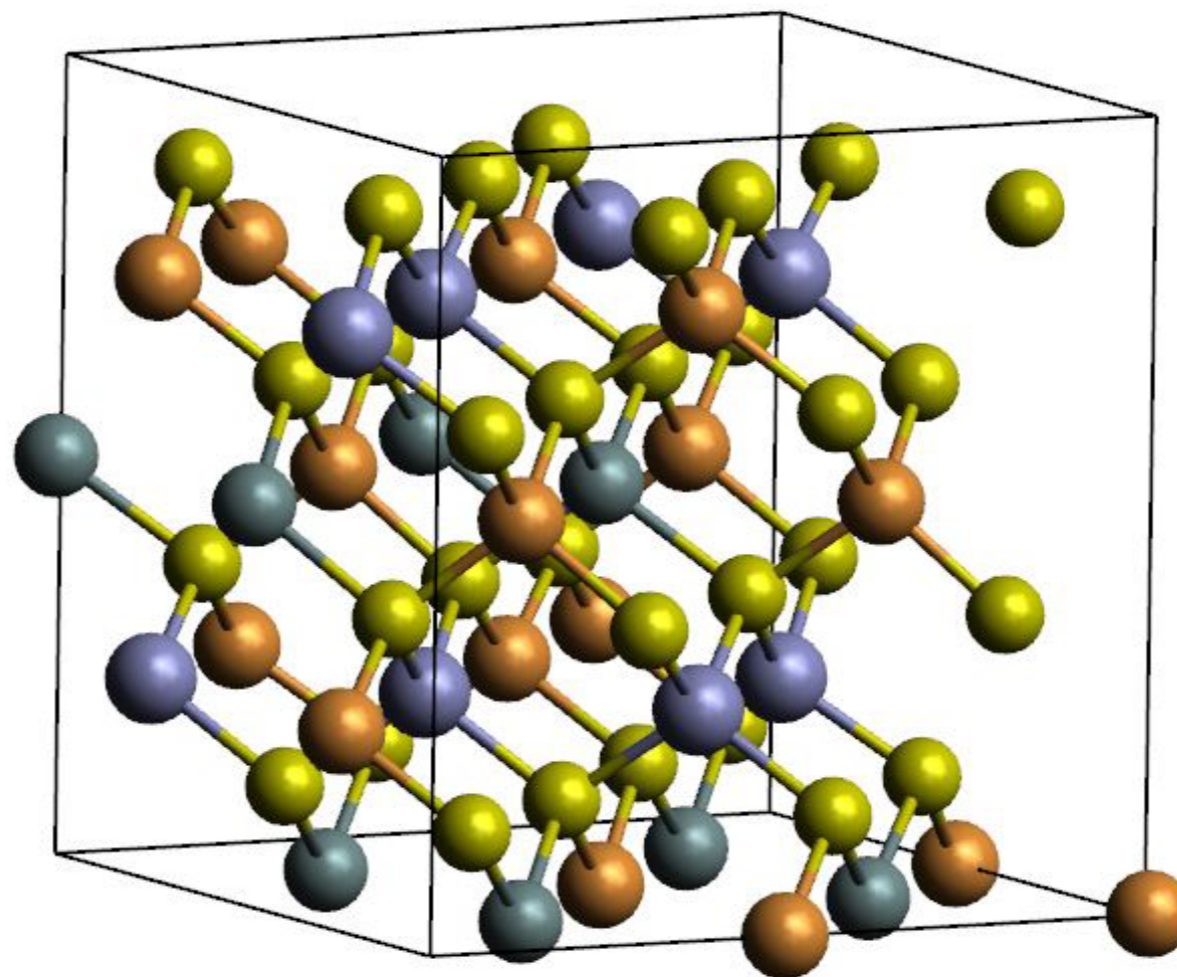
18 (34) Ritscher, A.; Hoelzel, M.; Lerch, M. The Order-Disorder Transition in Cu<sub>2</sub>ZnSnS<sub>4</sub> – A  
19 Neutron Scattering Investigation. *J. Solid State Chem.* **2016**, 238.  
20 <https://doi.org/10.1016/j.jssc.2016.03.013>.  
21  
22  
23  
24  
25  
26  
27  
28  
29  
30  
31  
32  
33  
34  
35  
36  
37  
38  
39  
40  
41  
42  
43  
44  
45  
46  
47  
48  
49  
50  
51  
52  
53  
54  
55  
56  
57  
58  
59  
60





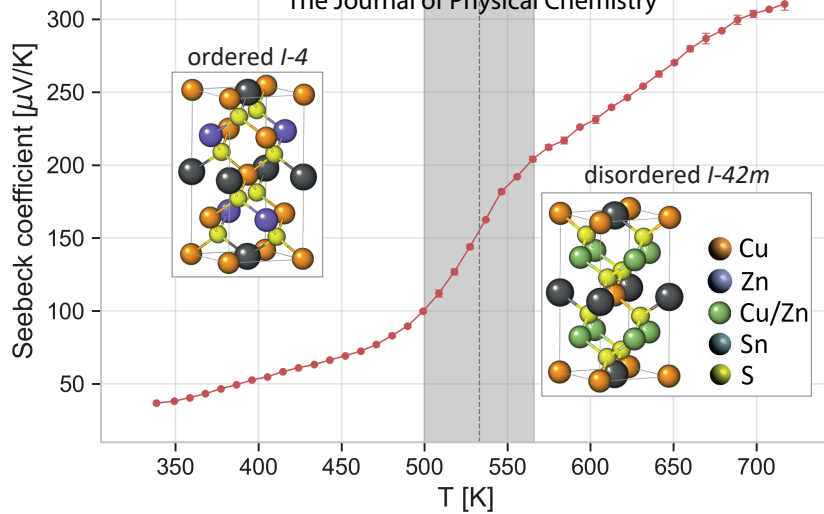
1  
2  
3  
4  
5  
6  
7  
8  
9  
10  
11  
12  
13  
14  
15  
16  
17  
18  
19  
20  
21  
22  
23  
24  
25  
26  
27  
28  
29  
30  
31  
32  
33  
34  
35  
36  
37  
38  
39  
40  
41  
42  
43  
44  
45  
46  
47  
48  
49  
50  
51  
52  
53  
54  
55



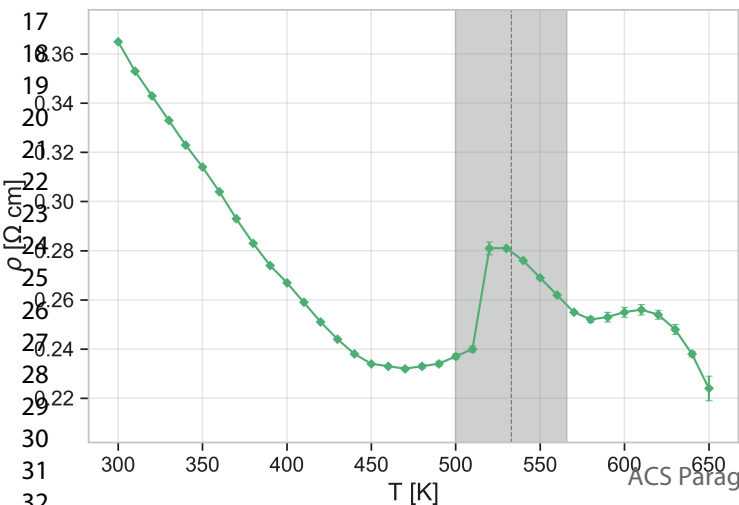
**a****b**

ACS Paragon Plus Environment

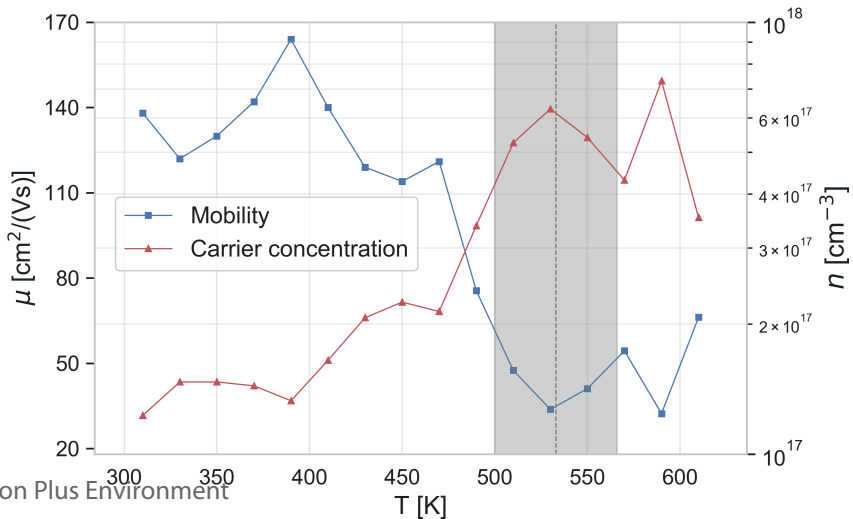




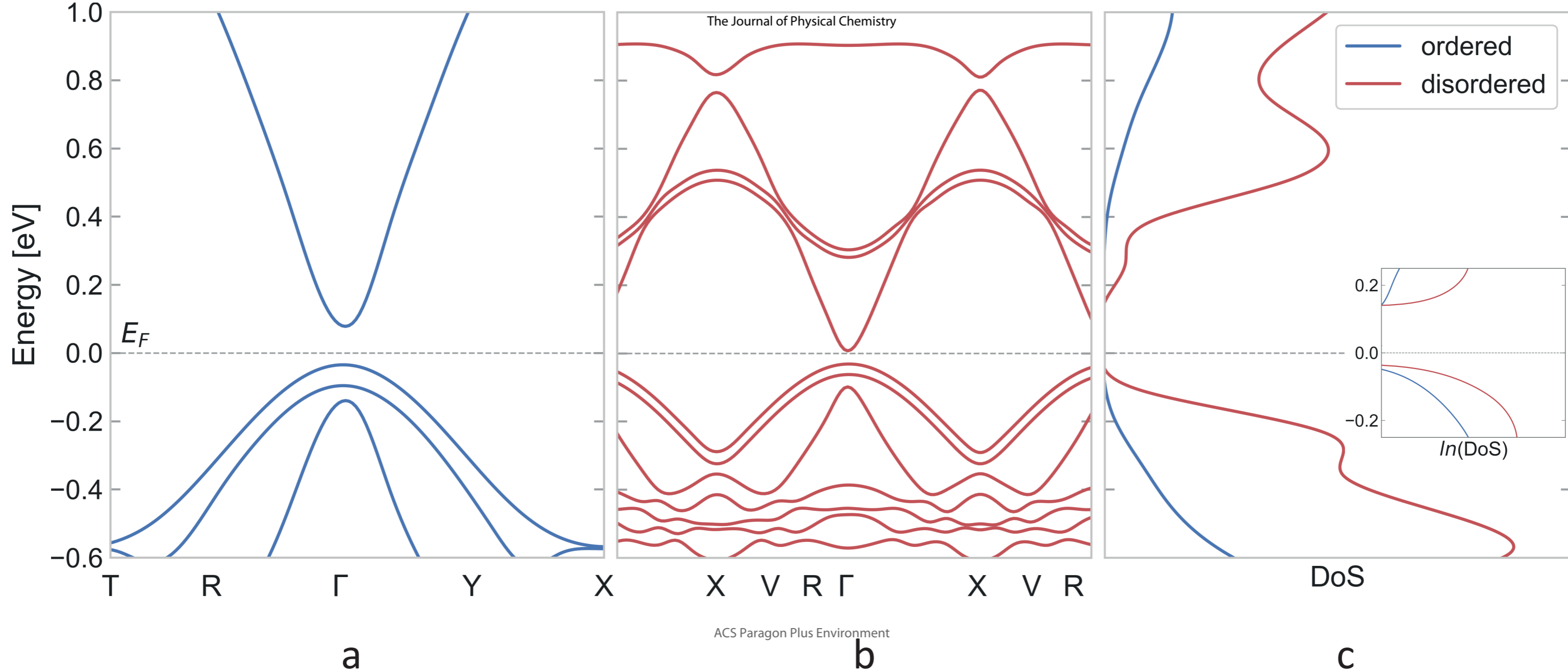
a

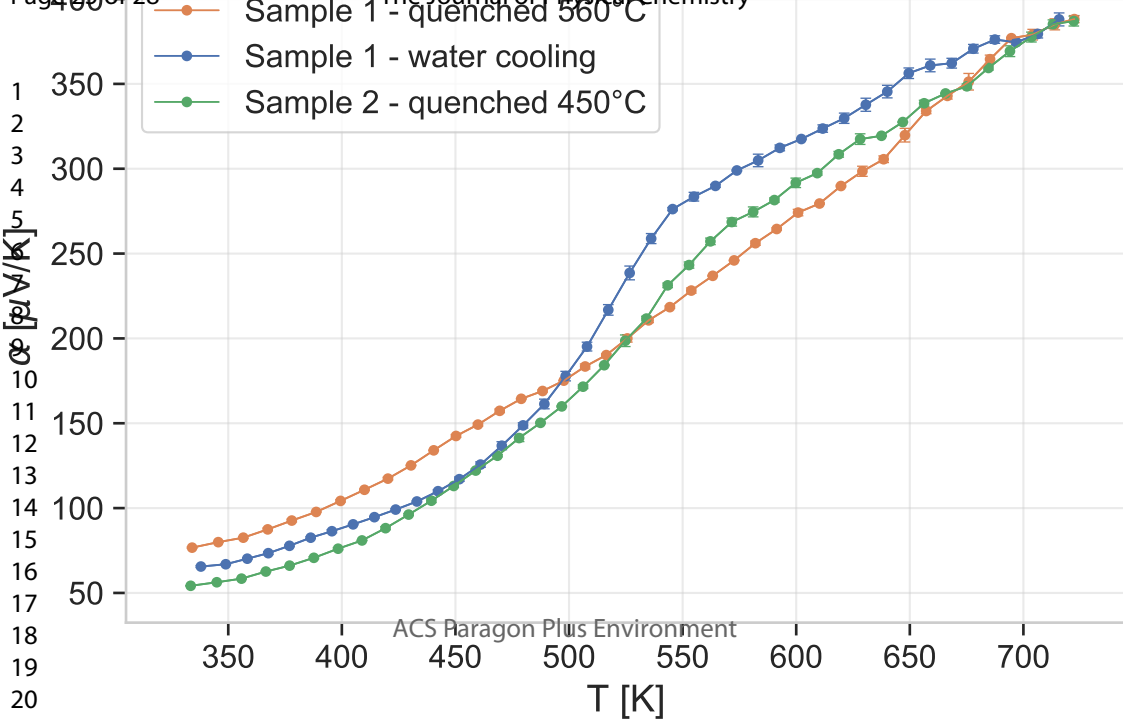


b

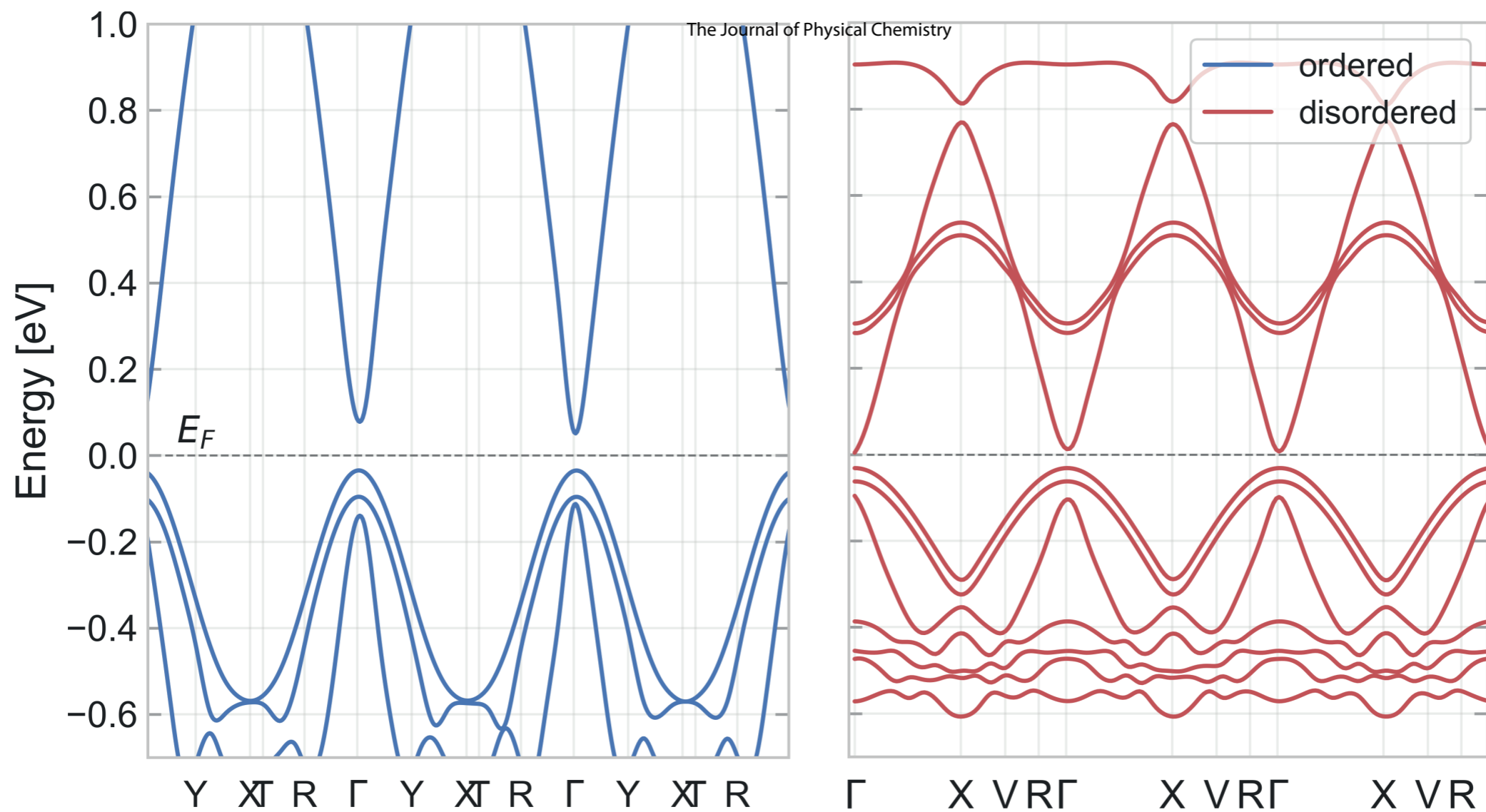


c







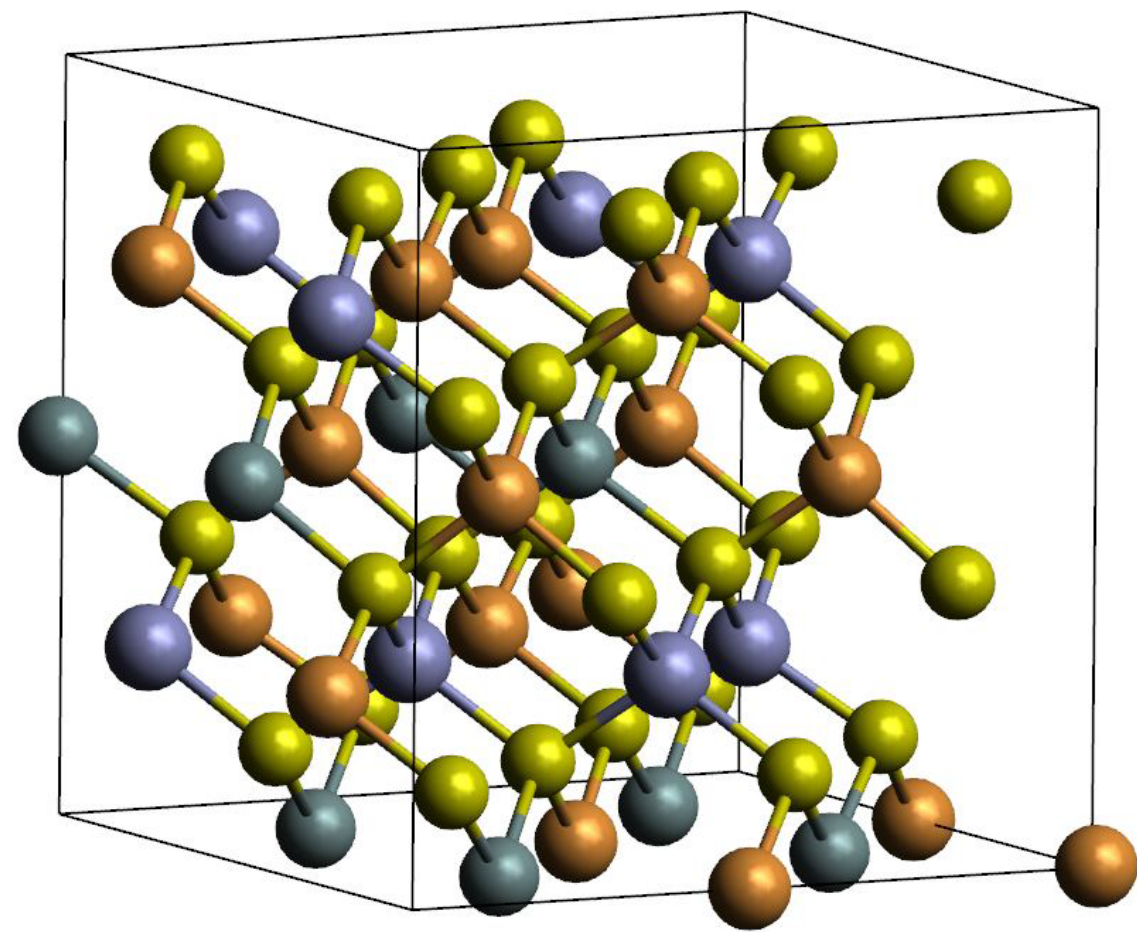


a

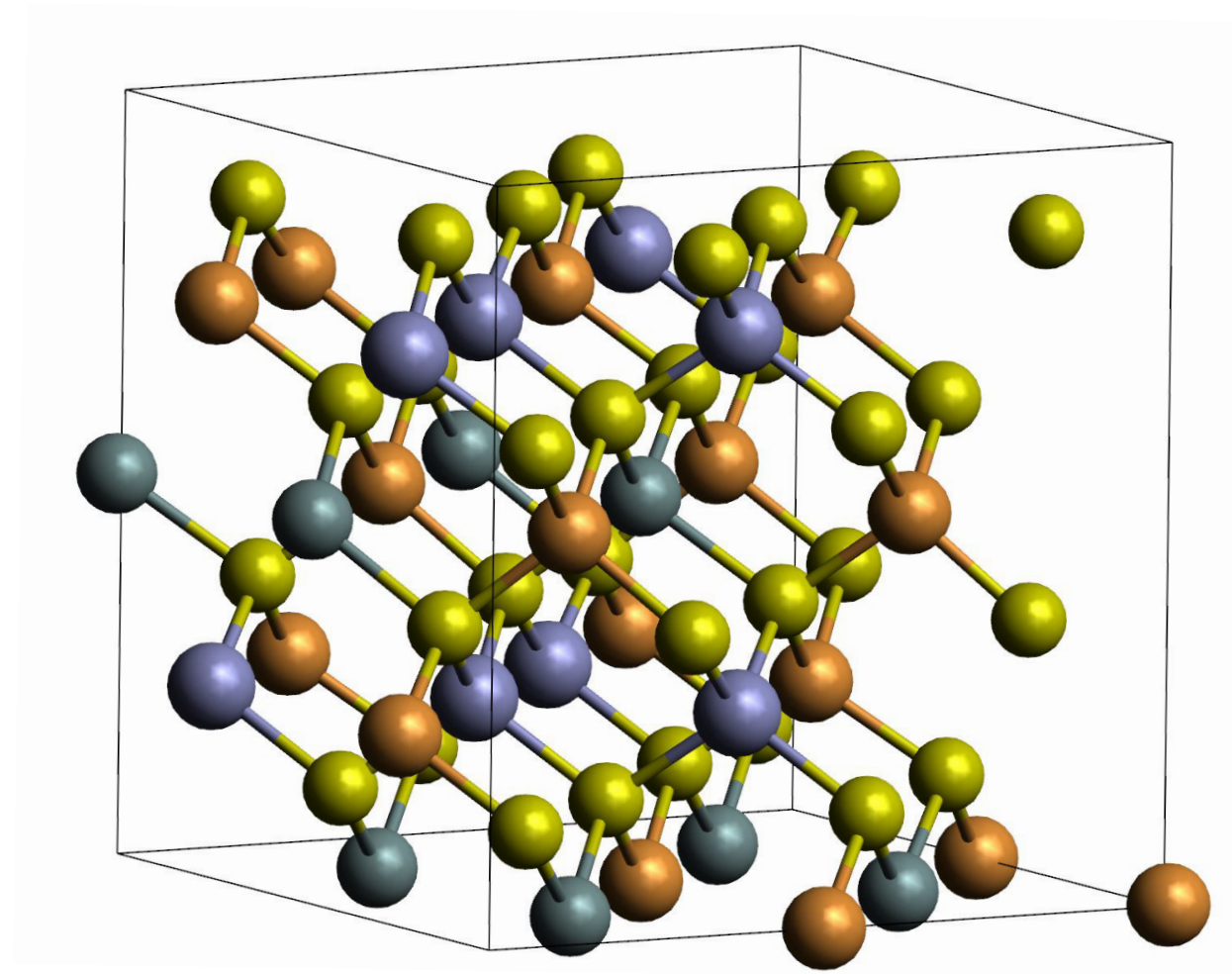
ACS Paragon Plus Environment

b

1  
2  
3  
4  
5  
6  
7  
8  
9  
10  
11  
12  
13  
14  
15  
16  
17  
18  
19  
20  
21  
22  
23  
24  
25  
26  
27  
28  
29  
30  
31  
32  
33  
34  
35  
36  
37  
38



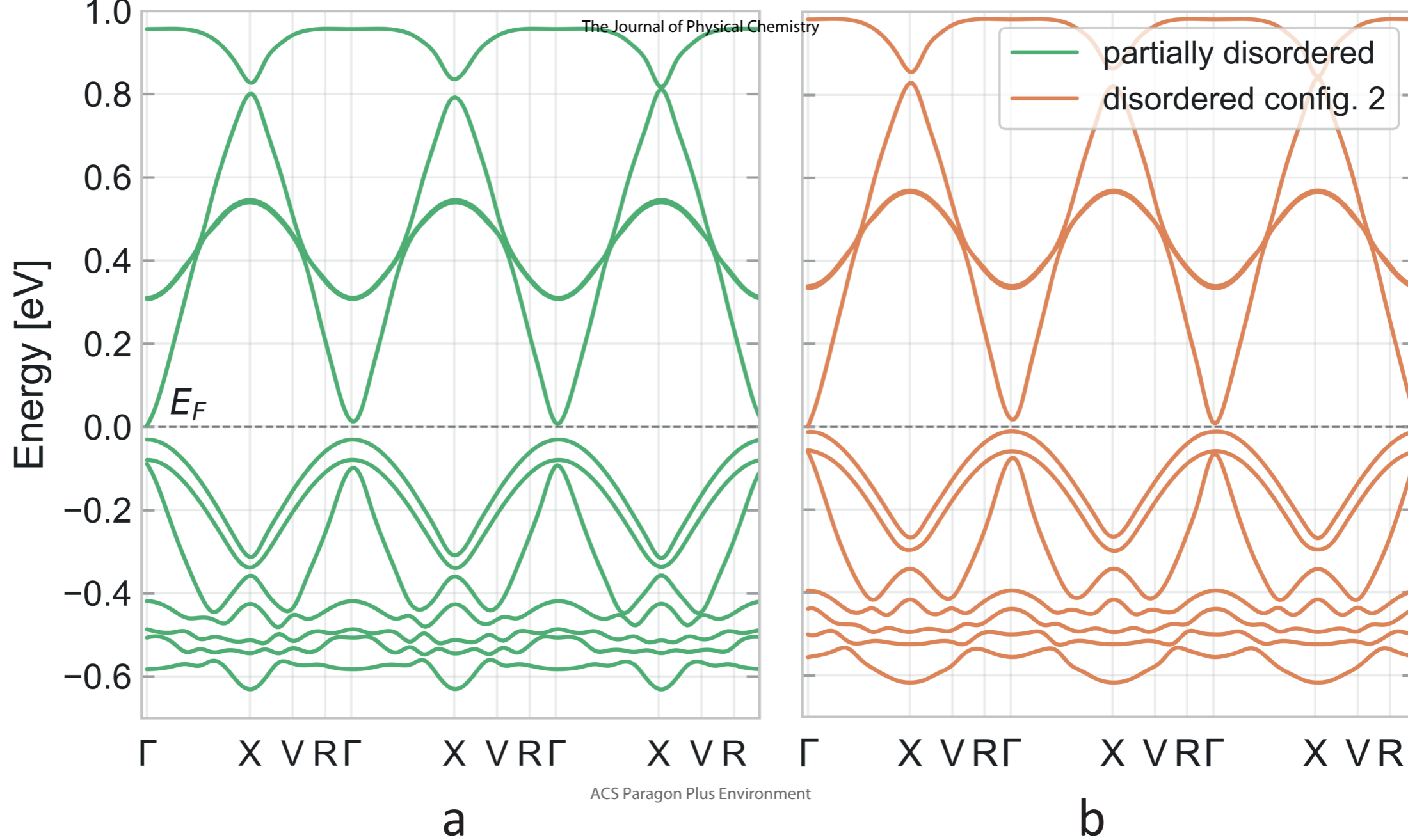
a



b





1  
2  
3  
4  
5  
6  
7  
8  
9  
10  
11  
12  
13  
14  
15  
16  
17  
18  
19  
20  
21  
22  
23  
24  
25  
26  
27  
28  
29  
30  
31  
32  
33  
34  
35  
36  
37  
38